PAPER

Check for updates

Unlocking long-term stability in metal-based gas diffusion electrodes for CO$_2$ electroreduction

Chandani Singh, [iD] †[a] Jia Song, [iD] †[a] Ranjith Prasannachandran, [iD] [a]
Asier Grijalvo, [iD] [a] Jing Shen,[a] Zhiyuan Chen, [iD] [a] Jan Vaes, [iD] [a] Yuvraj Y. Birdja [iD] *[a]
and Deepak Pant [iD] *[ab]

Electrochemical CO$_2$ reduction (ECR) to formate/formic acid (FA) represents one of the most viable pathways for converting CO$_2$ into value-added chemicals, particularly under industrially relevant conditions. However, long-term operational stability of gas diffusion electrodes (GDEs) at high current densities remains a critical bottleneck. Herein, we report the development of carbon-free bismuth (Bi) and tin (Sn)-based GDEs fabricated *via* a custom methodology that enables stable ECR operation for over 4000 hours (Bi) and 1050 hours (Sn) at 100 mA cm^{-2}, achieving faradaic efficiencies (FE) of up to 90% and 70%, respectively. A comprehensive mechanistic investigation reveals that performance degradation is predominantly driven by dynamic changes in the bulk catholyte, particularly pH shifts and HCO$_3^-$ ionic depletion, rather than intrinsic catalyst decay. Control experiments and *in situ* Raman spectroscopy highlight the formation and regeneration of bismuth subcarbonate species as key intermediates in the ECR process. The results demonstrate sustained operation with periodic reactivation, rather than static stability, highlighting how electrolyte management and pulsed electrolysis can extend system durability under industrially relevant conditions. Crucially, we demonstrate that a combination of catholyte refreshment and periodic anodic pulsing reactivates electrode performance, sustaining high selectivity and suppressing the hydrogen evolution reaction (HER) over extended durations.

Broader context

Climate change and global energy insecurity demand urgent and sustainable solutions that reduce greenhouse gas emissions while meeting growing industrial needs. Electrochemical conversion of carbon dioxide (CO$_2$) into value-added chemicals and fuels offers a promising route to close the carbon loop—especially when powered by renewable electricity. Among the possible products, formate and formic acid are particularly attractive due to their roles in chemical synthesis, hydrogen storage, and energy applications. However, one of the major challenges in scaling up CO$_2$ electrolysis is the lack of long-term electrode stability at high current densities, which is essential for industrial implementation. This study tackles the critical issue of electrode degradation by developing robust, carbon-free gas diffusion electrodes made from tin and bismuth. Our system operates stably for over 4000 hours—more than doubling the duration of previously reported technologies—while maintaining high selectivity for formate production. We identify degradation mechanisms rooted in changes to the electrolyte, rather than the catalyst itself, and introduce an effective, scalable reactivation strategy using periodic anodic pulses. These findings move electrochemical CO$_2$ conversion technologies closer to commercial deployment, with broad implications for reducing fossil fuel dependency, enabling circular carbon economies, and advancing global carbon management strategies.

Introduction

CO$_2$ conversion and utilization (CCU) is a promising strategy for mitigating greenhouse gas emissions and reducing the carbon footprint. As global warming and climate change are primarily driven by increased atmospheric CO$_2$, CCU is expected to play a vital role in addressing these challenges.[1] Among various CCU methods, electrochemical CO$_2$ reduction (ECR) stands out as a key technology when powered by renewable energy sources. The products obtained from ECR play a pivotal role as a chemical feedstock,[2] such as carbon monoxide,[3] organic acids (such as formic acid and acetic acid),[4,5] alcohols (such as methanol and ethanol)[6] and hydrocarbons (such as methane and ethylene).[7] The general approach with ECR is using a gas diffusion electrode (GDE) in a flow cell set-up. This design

[a] *Electrochemistry Excellence Centre, Material and Chemistry (MatCh) Unit, Flemish Institute for Technological Research (VITO), Boeretang 200, 2400 Mol, Belgium. E-mail: yuvraj.birdja@vito.be, deepak.pant@vito.be*

[b] *Center for Advanced Process Technology for Urban Resource Recovery (CAPTURE), Frieda Saeystraat 1, 9000 Gent, Belgium*

† Equal contribution.

addresses the limitations of CO_2 solubility and mass transport typically observed in H-cell setups. GDE-based flow cells create a three-phase solid–liquid–gas interface at the catalyst surface, enhancing CO_2 utilization efficiency and product yield by reducing CO_2 waste.[8] The commercially available GDEs predominantly comprise carbon-based electrodes with electrocatalysts immobilized on porous carbon supports.[9] However, most ECR experiments using GDEs have focused on short-term performance, typically ranging from a few hours to a few days.[10,11] Metal-based electrocatalysts, such as tin (Sn) and bismuth (Bi), are favoured for their high catalytic activity and selectivity towards formate production.[12] The role of Sn and Bi in ECR is well documented for their selectivity towards formate/formic acid (FA), (N.B. FA represents both formate and formic acid if not explicitly stated).[13,14] Still, the long-term operation at industrially relevant current density has been limited.[2,14–17] Despite numerous studies demonstrating the efficacy of high-temperature solid oxide electrolyser cells (SOECs) for CO_2 electroreduction, a notable gap exists in the literature regarding long-term low-temperature ECR.[18]

Sn as an electrocatalyst is widely used, but in majority of the studies, it is in the form of ink by spray coating or inking on a support.[11,19,20] The studies so far have reported issues such as catalyst leaching, agglomeration, poisoning and Ostwald ripening as the reason for catalyst degradation.[13] There are only a few reports with large-scale operations with higher current density and higher FE (range 60–80%).[15] Yang et al.[21] demonstrated the novel, three compartment flow cell for direct collection of formic acid. The authors reported operational stability of 500 h at a current density of 140 mA cm^{-2}. Li et al. reported a Sn-Bi/SnO$_2$ active catalyst in situ synthesized on uniformly alloyed Bi$_{0.1}$Sn surface allowing efficiently reducing CO_2 to formate over 100 days (2400 h) achieving 95% faradaic efficiency (FE) towards FA.[22] Computational studies established the role of Bi optimizing the reaction energy, suppressing unwanted by-products like CO and H$_2$ and maintaining high catalyst stability. This report is a rare example of extended operation, underscoring how uncommon long-term stability results are. This approach stabilized the electrode for operation for 2400 h at 100 mA cm^{-2}.

Despite these advancements, achieving industrially relevant long-term stability remains a significant challenge.[23–27] In this work, we have incorporated a simple yet efficient method to produce carbon-free metal GDEs (namely Bi and Sn GDE), with tailor-made properties and dimensions that can be adapted to the cell configuration or experimental conditions (e.g. including a current collector and a hydrophobic GDL).[28] Notably, Bi-based electrodes operate effectively at a current density of 100 mA cm^{-2} for over 4000 hours, maintaining a FE of 85%. Our work explores process modifications that extend operational duration and enhance catalyst stability, including factors such as membrane type, electrolyte concentration, and the implementation of an electrochemical pulsing technique. In contrast to previous reports that primarily addressed extended operation time or selectivity modulation, this study identifies the physicochemical origins of degradation and introduces anodic pulsing as a reactivation tool for metal-based CO_2RR electrodes, validated by in situ Raman spectroscopy and long-term operation exceeding 4000 h.

Results and discussions

To address the stability limitations in electrochemical CO_2 reduction (ECR), we developed self-supporting, carbon-free gas diffusion electrodes (GDEs) composed of bismuth (Bi) and tin (Sn). These electrodes were tested at an industrially relevant current density of 100 mA cm^{-2}, achieving extended operation times of up to 4000 hours for Bi and 1050 hours for Sn under continuous flow-cell conditions. Detailed fabrication protocols and the electrolyser configuration are provided in the SI (Sections S1.1–S1.2 and Fig. S1). Unlike conventional carbon-supported GDEs that may suffer from corrosion and competing hydrogen evolution reaction (HER) under cathodic bias, the carbon-free design integrates the catalytic and gas diffusion layers into a single metallic matrix. This configuration maximizes utilization of active sites, eliminates catalyst detachment, and enables long-term operational stability over thousands of hours (EP4182491B1).[28] The central focus of this work lies in the elucidation of electrode degradation and subsequent performance recovery via a pulsed electrolysis strategy, which enabled stable long-term operation. In situ Raman studies were carried to understand further the factors causing the revival of the electrode, discussed later in this section. The stability of electrodes is due to the GDE production method and modification of key parameters during the electrocatalytic process. Initial electrode preparation required an electrochemical activation step, functioning as a sintering process to enhance conductivity (Section S1.3). Scanning electron microscopy (SEM) revealed clear morphological changes between pristine and activated GDEs (Fig. S2 and S3), confirming microstructural evolution. As shown in Fig. S4, linear sweep voltammetry (LSV) confirms a substantial increase in current density after activation, directly evidencing the improved electrical conductivity and reduced in-plane resistance of the GDE.

The freshly activated GDEs were used for the electrochemical performance testing of ECR. The electrochemical cells with Sn and Bi GDE as cathodes were operated in galvanostatic mode at 100 mA cm^{-2} for 1050 h and 4000 h, respectively. Faradaic efficiency (FE) towards FA was used as an indicator to monitor the electrocatalytic performance of the electrode, which is proportional to the partial current density for galvanostatic processes and reported to be the key performance metric for stability studies of ECR.[23] Online gas chromatography continuously monitored the CO and H$_2$ produced during the cell operations. Here, we established a correlation between variation in the property of bulk electrolyte and the electrode activity with ECR. The initial 1000 hours are included in this discussion to streamline the analysis. The total operational time is divided into three distinct zones based on its selectivity towards FA, providing further insight into the process. These zones are observed in all the reproduced experiments for both electrodes and depicted schematically in Fig. 1. These zones are, namely, [I] The stability zone ($\approx$0–200 h of operation); [II] The degradation zone ($\approx$200–400 h); [III] The reactivation zone (beyond 400 h).
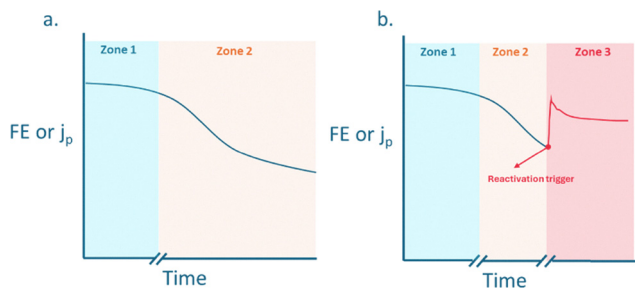
Fig. 1 Schematics of different zones in terms of FE(FA) with respect to time (a) without any reactivation trigger (b) with reactivation trigger.

[I] The stability zone (0–200 h)

Both Bi and Sn GDEs exhibited stable electrochemical performance towards FA production during the initial 0–200 hours (Fig. 2 and Fig. S5). The negligible changes observed in the electrocatalytic behaviour of the electrodes during this period led to its designation as "stability zone". While the term "stability" may not fully encapsulate the actual stability of the electrodes, it was chosen to help clarify the minor fluctuations that occurred in the electrolyser over this operational window. During this zone, we observed that Sn GDE as cathode had FE_{FA} 70–75%, 5–6% FE_{CO} and HER accounts for 20–25% of FE (Fig. S5). A similar trend was observed for Bi-GDE, with a higher selectivity towards FA resulting in FE_{FA} of 85–90% (Fig. 2). The datasets presented in Fig. 2–6 originate from the same continuous long-term experiment unless stated otherwise. Bi GDE long-term data were complemented with shorter duplicate runs confirming reproducibility. Specifically, the control experiment in Fig. 4, conducted in 0.5 M KHCO$_3$ at 100 mA cm^{-2}, shows an initial FE_{FA} that differs by <10% from the recovered FE_{FA} observed after pulsing in the long-term stability experiments shown in Fig. 2a and 6.

Recently, Fernández-Caso et al.[14] reviewed the recent developments and shortcomings in scaling up electrochemical CO$_2$ reduction to FA. While Sn and Bi-based catalysts are predominantly reported, studies demonstrating stability beyond 500 h are scarce. In another study, Mila et al.,[16] compared the performance of Sn and Bi-based GDEs. Although a high FE_{FA} (94.2%) at 200 mA cm^{-2} was reported, operational duration was limited to 200 hours, highlighting a lack of long-term stability. Moreover, electrodes prepared by the pulse plating method showed stability for only 23 hours before metal leaching was observed, compromising the catalyst's integrity. These findings underscore the need for improved GDE designs, which we address in the current work. The approach adopted here resulted in negligible metal leaching even after prolonged operation (i.e., >1000 hours), (SI, Section 2.1).

Fig. 2a illustrates the initial 300 hours of electrolysis with Bi GDE as the working electrode. Here, the FE_{FA} is calculated via two methods: (1) direct measurement of accumulated FA concentration in the catholyte using high-performance liquid chromatography (HPLC) (represented as black dots in Fig. 2a), (2) derived from the gas chromatography (GC) analysis for CO and H$_2$ from the exit gas of the cathode correlated by Eqn 1 (FE of each product is represented by shaded region; green for H$_2$, blue for CO and light blue shaded region is FA), as there is no trace of any other byproduct from the ECR using the Bi or Sn electrode. No additional carbon-containing products were detected by GC or HPLC, confirming that the loss in apparent FE arises from measurement protocol and ionic transport rather than parasitic reactions. As expected, progressive accumulation of formate in the catholyte led to measurable changes in both bulk conductivity and bulk pH over time, consistent with the trends observed in Fig. 2b and c. Note that we refer to bulk pH when mentioning pH unless explicitly mentioned local pH. To clarify the relationship between concentration buildup and FE_{FA}, the underlying numerical data for the first 250 h, including sampling intervals, FA concentrations, catholyte volumes, and calculated FE_{FA} are presented in Table S1. These values confirm that FA accumulation is not strictly linear and that the observed trends are fully consistent with the declining FE_{FA} obtained from both gas and liquid analyses.
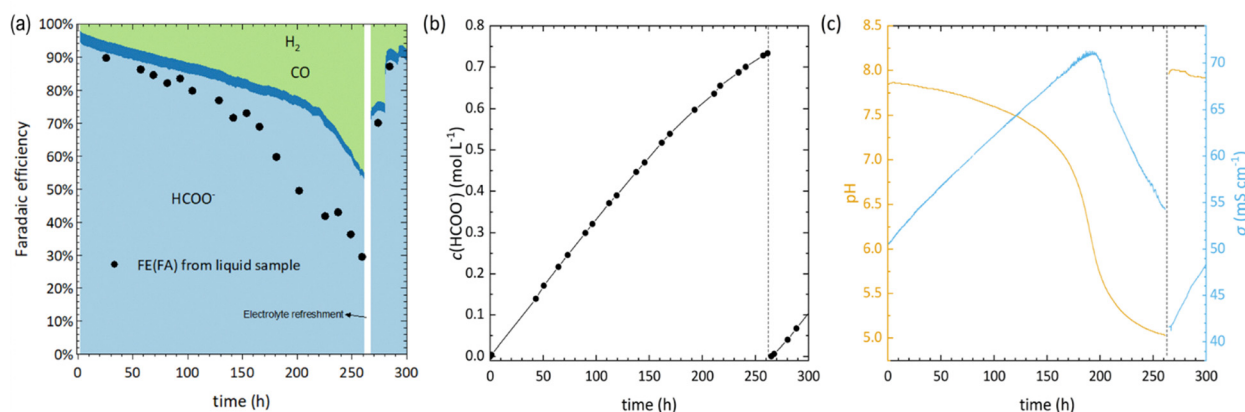
$$FE_{FA} = 100\% - FE_{CO} - FE_{H_2} \tag{1}$$

Fig. 2 The initial 300 hours of Bi GDE at 100 mA cm^{-2}, depicting the stability and degradation zones, during which process the change of (a) faradaic efficiency of products, (b) HCOO$^-$ concentration in the catholyte, and (c) pH (left y-axis) and conductivity (right y-axis) of the catholyte are plotted against time. Data shown are from the same continuous experiment.
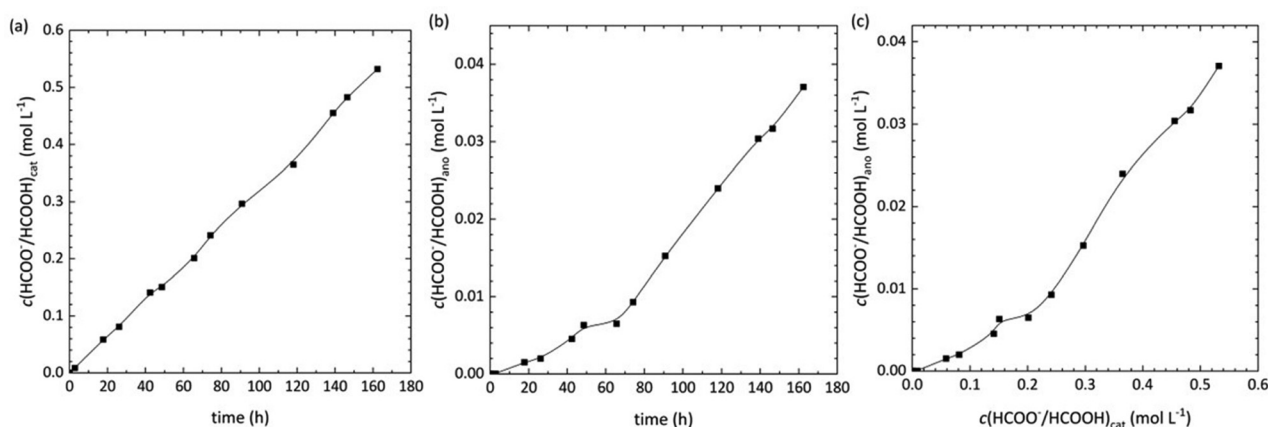
Fig. 3 Time-dependent formate concentrations in the (a) catholyte and (b) anolyte during long-term electrolysis with Bi GDE at 100 mA cm^{-2}, demonstrating crossover through the bipolar membrane contributing to differences between GC- and HPLC-derived faradaic efficiencies (*cf.* Fig. 2a). (c) The FA concentration in the anolyte is plotted against that in the catholyte. Data shown are from the same continuous experiment.

Importantly, the custom-engineered structure of our GDEs mitigates one of the most common degradation pathways in gas-fed systems: flooding of the GDL due to salt precipitation. This is achieved by incorporating a spatially defined separation between hydrophilic and hydrophobic regions within the porous electrode, thereby preserving CO_2 access to the catalyst layer (CL) and maintaining gas–liquid–solid interfacial integrity. Despite this structural advantage, a noticeable sharp decline in catalytic performance was observed beyond 200 hours of continuous operation, marking the onset of the next zone, "the degradation zone".

In Fig. 2a, an increasing discrepancy is observed between the FE_{FA} calculated from liquid samples (black circles) and that derived from gas samples (shaded light blue region) as a function of time, which can be associated with an increase in $HCOO^-$ concentration. Although bipolar membranes (BPMs) typically suppress ionic crossover, the observed FA presence in the anolyte is associated with electroosmotic drag, which is influenced by the changes in the catholyte property, namely HCO_3^- depletion, acid accumulation, and pH drop.[29,30] The sharp divergence in FE after $\sim$150 h, coinciding with high FA concentration and proton buildup, suggests ionic shifts and increased HCOOH permeability, driving the observed discrepancies in FA concentration in the catholyte. A control experiment was conducted to monitor the change of $HCOO^-$/HCOOH concentration in the catholyte, the details of which are mentioned later in the degradation zone. In Fig. 3, it can be observed that as the $HCOO^-$ accumulates in the catholyte, the $HCOO^-$ concentration in the anolyte starts to ramp up, and the crossover rate noticeably accelerates as the accumulated concentration of $HCOO^-$ increases in the catholyte. Consequently, the FE_{FA} calculated from the measurement of liquid product in the catholyte is an underestimation as the $HCOO^-$ concentration increases above 0.5 M. Therefore, the FE_{FA} referred to in this article will be primarily based on the GC analyses following eqn (1).

[II] The degradation zone ($\approx$200–400 h)

Following the initial stability phase, a pronounced decline in the faradaic efficiency towards formate (FE_{FA}) is observed, which marks the onset of the "degradation zone" (Fig. 2a). This transition occurs between 200–260 h for the Bi GDE and 200–350 h for the Sn GDE (Fig. 2a and Fig. S5e, respectively), with the discrepancy attributed to differences in the rate of formate accumulation within the catholyte reservoir. This accumulation perturbs both the pH and conductivity of the bulk electrolyte, leading to a condition-dependent shift in system behaviour. As a result, the duration of each zone is not fixed and depends on the experimental conditions. These changes in the catholyte gradually result in transitions from ECR to the competitive HER for both electrodes. As illustrated in Fig. 2c, the pH evolves with a sigmoidal profile, while conductivity exhibits an inverted V-shaped trend, both indicative of significant changes in catholyte composition. Comparable behaviour was observed for the Sn GDE (Fig. S5f). For the Bi GDE, the evolution of the working-electrode potential (E_{we} *vs.* Ag/AgCl) and the overall cell voltage during long-term operation is shown in Fig. S6. Both traces gradually drift to more negative potentials/higher cell voltages upon entering the degradation zone, consistent with the conductivity loss and pH changes discussed in Fig. 2c. These results suggest that the selectivity of ECR, in this case, is more strongly related to the composition of the catholyte than to the intrinsic deactivation of the electrodes. The changes in pH and conductance of the catholyte are linked to the formation of potassium formate, which, with continuous production, gradually depletes the HCO_3^- ions and leads to the accumulation of formic acid. As the concentration of HCOOH increases in the catholyte, both pH and conductance decrease, affecting the selectivity of Sn and Bi GDEs towards formic acid production. The interplay between pH and the formate/formic acid equilibrium critically governs this transition. While a moderate decrease in pH initially supports formic acid formation and limits carbonate precipitation, further acidification (pH < 6) enhances proton activity,
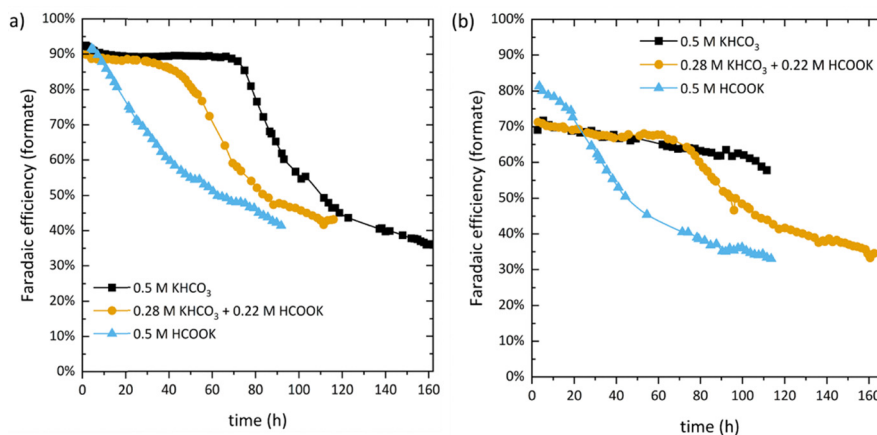
Fig. 4 Time dependent evolution of the FE (HCOO⁻/HCOOH) in a series of long-term control experiments with a current density of 100 mA cm⁻² and changing the catholyte composition while using (a) Bi GDE; and (b) Sn GDE as cathode.

favouring HER and leading to selectivity loss. The degradation zone thus reflects the collapse of the buffer capacity rather than intrinsic catalyst deactivation.

To further investigate the degradation mechanism(s), control experiments were conducted to study the influence of (1) proton concentration (pH) and (2) the impact of the accumulation of formate in the catholyte selectivity of the GDEs. In these experiments, the electrolyte, cathode, and membrane were consistent with those used in the long-term experiment (Table 1). Ni (planar electrode) was chosen as an anode due to its relatively low catalytic activity towards formate/formic acid electro-oxidation reaction.[31]

As shown in Fig. 4a, at $t \approx 0$, $FE_{FA} \approx 90\%$ across electrolytes without added HCOOH, indicating no immediate evidence of formate-induced poisoning under buffered conditions. The subsequent FE evolution differs across electrolytes due to bulk-electrolyte changes (pH and conductivity), not due to the initial presence of HCOO⁻. This uniformity suggests that formate ions do not negatively impact on the catalytic activity for ECR, for instance, *via* surface poisoning. Although the equilibrium between formate and formic acid is always present, the measured pH values (6.5–8.2) indicate that >99% of the dissolved carbon species exist as HCOO⁻. Therefore, the contribution of molecular HCOOH to the initial composition is negligible. A similar trend is observed for the Sn GDE (Fig. 4b), although with a lower initial FE_{FA} of approximately 75 ± 5%, indicating inherent material differences in catalytic performance. However, the time evolution of FE_{FA} varies significantly with electrolyte composition. Two distinct modes of performance degradation are evident, as inferred from the differing

slopes in the decline of FE following the initiation of electrolysis. The first degradation mode is likely linked to the accumulation of formic acid, which increases proton concentration and enhances the hydrogen evolution reaction (HER). The first degradation mode is therefore linked to increasing proton activity as pH declines (buffer exhaustion/K⁺ depletion), which promotes HER; it is not inferred from the initial presence of HCOO⁻. The second mode appears to be associated with salt precipitation or buildup during the ECR process, which gradually obstructs the GDE pores and leads to a progressive loss in catalytic efficiency.[32–34]

The time-dependent profiles of FE_{FA} and FE_{H2} in a 0.5 M KHCO₃ catholyte were plotted alongside the corresponding changes in proton concentration (Fig. 5). Notably, the rise in FE_{H2} closely parallels the increase in proton concentration, which is attributed to the accumulation of formic acid (HCOOH). Once the pH of the catholyte drops below the effective buffering range of the carbonic acid–bicarbonate system, the bicarbonate
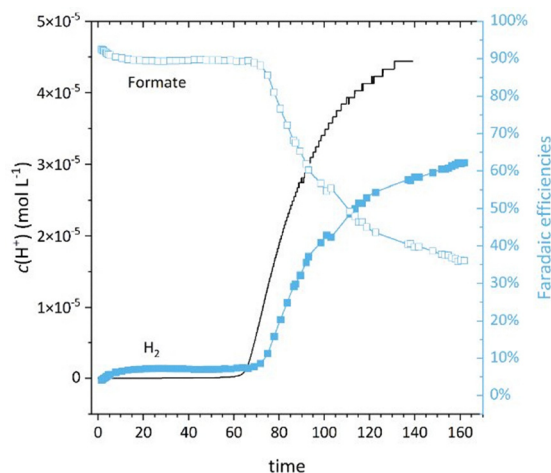
Table 1 The catholyte composition used for control experiments

Composition	Solution 1	Solution 2	Solution 3
KHCO₃	0.5 M	0.28 M	0 M
HCOOK	0 M	0.22 M	0.5 M
HCOOH	0 M	0 M	0 M
Measured pH (before electrolysis)	7.6	7.43	6.25

Fig. 5 Time dependence of proton concentration in the catholyte (left y-axis) and faradaic efficiencies towards formate and H₂ (right y-axis) in an ECR experiment in 0.5 M KHCO₃ catholyte solution and 100 mA cm⁻².
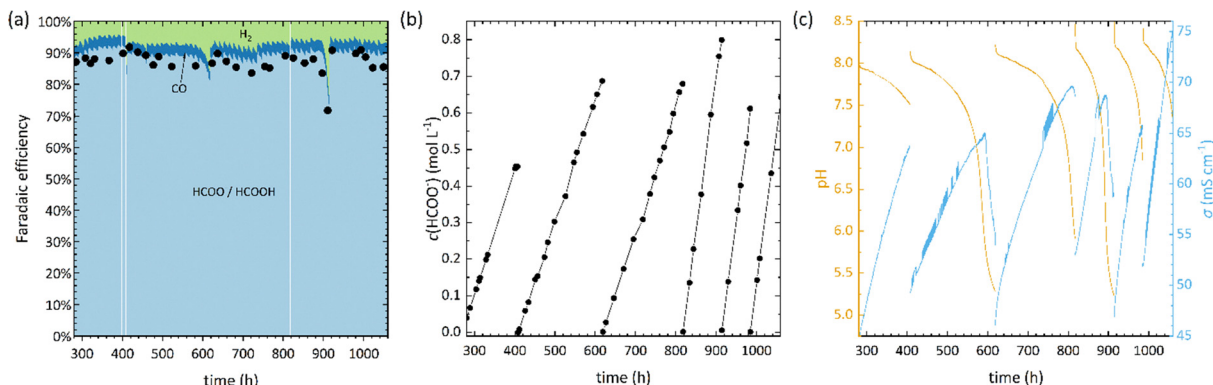
Fig. 6 Reactivation Zone: continuous operation from 275–1075 hours of Bi GDE at 100 mA cm^{-2}, with evolution over time of (a) faradaic efficiency of products, (b) formate concentration in the catholyte reservoir, and (c) pH (left) and conductivity (right) of the catholyte. Data shown are from the same continuous experiment.

ions (HCO$_3^-$) are gradually replaced with formate ions, primarily as potassium formate (HCOOK). Upon the exhaustion of HCO$_3^-$ ions through neutralization with protons generated at the BPM interface, the buffer capacity collapses, leading to a further decrease in pH. This correlation indicates that the decline in formate selectivity observed after approximately 70 hours primarily arises from the elevated proton concentration caused by HCOOH formation, which in turn promotes the HER. These findings underscore the importance of maintaining an adequate supply of KHCO$_3$ to the catholyte to prevent HCO$_3^-$ depletion and preserve the buffering capacity, thereby sustaining high selectivity toward formate during electrochemical CO$_2$ reduction (ECR). The control experiments attributed the changes in the catholyte as the major contributor to the shift in selectivity from ECR to HER. To restore the selectivity towards FA, reactivation processes were introduced, as mentioned in the next part as "the reactivation zone".

[III] The reactivation zone (>400 h)

In this zone, the selectivity towards FA was re-established. Periodically refreshing the catholyte (Fig. 6), partially addresses this issue. For Bi GDE, this intervention increased FE$_{FA}$ from 55% to 75%, though its initial FE$_{FA}$ value was not fully recovered. A similar trend was observed for Sn GDE after refreshing the catholyte (Fig. S5e and S7). The pulsing strategy was systematically optimized using the Sn GDE, as summarized in Table S2, with pulse type and pulsing frequency identified as the key governing factors controlling catalyst regeneration and formate selectivity. The evolution of formate concentration in both catholyte and anolyte during long-term operation further confirms this interpretation. As shown in Fig. S8, formate accumulates continuously in the catholyte and a proportional increase is observed in the anolyte, demonstrating crossover through the BPM. This behaviour is consistent with the observed divergence between GC- and HPLC-derived FE values. Ineffectiveness to completely restore the selectivity of the catalyst to its initial value could be associated with intrinsic catalyst deactivation e.g. changes in the catalyst surface, oxidation state, electrode morphology or salt precipitation blocking the GDE pores, thereby decreasing electrocatalytic behaviour.

Although refreshing the electrolyte restores faradaic efficiency from ~55% to ~75%, the initial activity is not fully recovered. This suggests that, in addition to buffer capacity degradation, a gradual intrinsic deactivation of the metallic surface occurs over extended operation. SEM analysis after 4000 h (Fig. S9) shows localized coarsening and reduced surface coverage, consistent with literature reports of slow morphological evolution of Bi and Sn catalysts under prolonged CO$_2$ electroreduction.[32,34,35] The residual decline in FE observed after electrolyte refreshment is therefore attributed to mild, cumulative morphological changes of the Bi/Sn surface, an intrinsic catalyst effect, superimposed on the dominant process-induced degradation linked to electrolyte evolution.

In order to solve these issues, we resorted to the application of anodic pulses, which in the literature have been mainly used to steer the selectivity of ECR on copper electrodes.[7,36–42] Recent studies have reported the anodic pulse technique as one of the tools to solve the salt precipitation and influence the catalytic behaviour of various catalysts.[31,43–46] The introduction of anodic pulses in ECR has been reported, and their impacts vary with the applied frequency of the pulses. One such study reports the inclusion of anodic pulse as a self-cleaning agent, mitigating the carbonate salt formation, thereby avoiding the flooding of the GDE.[34,43] Chung et al. highlighted the technical and economic potential of pulsed CO$_2$ electrolysis, emphasising its ability to enhance catalyst stability and product selectivity through dynamic modulation.[44] Optimised pulse profiles could make this approach a viable alternative to conventional electrolysis. However, it is worth noting that economic viability varies case by case and involves a trade-off between optimised operational conditions and energy losses associated with the anodic pulses.

To restore and maintain the initial high selectivity towards formate, anodic pulsing was introduced as a reactivation strategy. The pulsing parameters were first optimised using the Sn-based GDE (Fig. S7) and subsequently applied to the Bi GDE system. The gradual FE$_{FA}$ increase observed during the pulsed-operation window (Fig. S7) arises from a synergy of short anodic pulses which clear surface adsorbates, alleviate carbonate salt accumulation and flooding, modulate local pH and
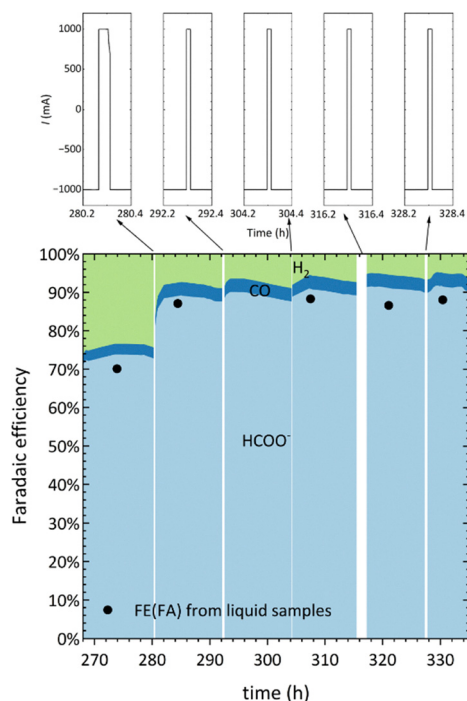
Fig. 7 Depiction of applied anodic pulses during CO_2 electrolysis with Bi GDE during the reactivation process.

cation fields, and concurrent bulk-electrolyte conditioning. In Bi, the pulses also regenerate subcarbonate species detected by in situ Raman, collectively restoring formate selectivity over time.[41,47–49] At 280 hours, a single anodic pulse of 30 seconds at 100 mA cm^{-2} was applied to the Bi electrode, resulting in a notable increase in FE_{FA} from 75% to 90% (Fig. 7). Following this, periodic anodic pulses of the same duration and current density were applied every 12 hours, successfully stabilising the formate selectivity over extended operation. Fig. 6 depicts the restoration FE_{FA} due to anodic pulsing for Bi GDE. During the initial 1075 hours of operation, a total volume of 21 L of 0.5 M $KHCO_3$ (refreshed 6 times with 3 batches of 5 L 0.5 M $KHCO_3$ and 3 batches of 2 L 0.5 M $KHCO_3$) was used to avoid the reduction of HCOOH selectivity due to pH decrease. A remarkable 90% selectivity to FA was maintained throughout the 1000 hours of electrolysis, suggesting that the combination of short anodic pulsing and catholyte refreshing can effectively maintain a high selectivity of the Bi GDE. Although formate/formic acid oxidation to CO_2 can occur under anodic conditions, the brief pulse durations relative to the cathodic phase rendered such losses negligible. Post-operation SEM images show morphological coarsening and partial densification of the surface after extended electrolysis, consistent with structural evolution under cathodic conditions (Fig. S9–S11). Post-mortem SEM/EDS analysis was conducted on the rinsed electrodes to examine surface morphology. Because the electrodes were washed with deionized water prior to analysis, residual $KHCO_3$ or HCOOK salts were removed, and quantitative detection of carbonate species was not possible. Under vacuum, remaining bicarbonate species tend to decompose, leading to possible

artifacts. No salt deposits or pore blockage were observed on the gas-facing side of the GDE, suggesting that flooding was minimal during operation.

Beyond 1075 hours (for Bi GDE), a gradual decline in FE_{FA} from 90% to 70% was recorded until 3700 hours, followed by a sharp drop in selectivity to 60% till 4000 hours, as shown in Fig. 8. A similar degradation trend was observed for the Sn GDE, as detailed in the SI (Fig. S7).

The frequent anodic pulsing aided in maintaining the pH near the electrode interface, reactivating the ECR reaction. The control experiments, coupled with pulsing electrochemical methods, are directed towards the association of metal carbonate species for the activation and deactivation process. To gain further insight into the pulsing process on the Bi electrode, in situ Raman studies were conducted. In situ Raman experiments were designed (SI, Section 1.4.2) for relevant experimental conditions from different zones for long-term ECR on a Bi GDE. Raman bands corresponding to CO_3^{2-}, HCO_3^-, and *COOH were mainly observed. However, the Raman bands at <200 cm^{-1} were of interest for the study since these are associated with the collective oxide entities of bismuth. At 165 cm^{-1}, a Raman band was detected that correlates with the so-called subcarbonate species as reported in the literature (Fig. 9).[50–56]

Evidently, during the electrocatalytic process, the surface of the Bi metal is surrounded by oxides, hydroxides, and carbonate ions. In situ Raman experiments provide evidence that Bi_xO_y spontaneously interacts with CO_2 or (bi)carbonate ions in the solution to generate $Bi_2O_2CO_3$. The changes of the Raman peak at 165 cm^{-1} at a reducing potential of -1.6 V vs. Ag/AgCl were monitored. The Raman peaks diminished over time and reappeared immediately after a positive potential of 2 V vs. Ag/AgCl was applied to the electrode. This confirms the formation of the subcarbonate species because of an anodic potential. This peak was also observed in an experiment with N_2-saturated
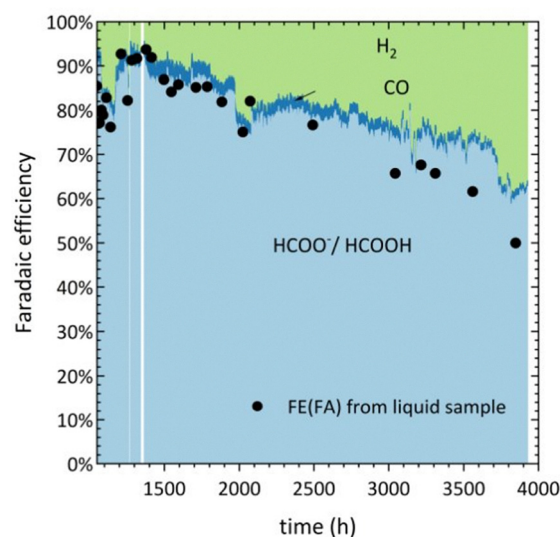

Fig. 8 Evolution of the FE after 1075 hours to 4000 hours of electrolysis with Bi GDE. Multiple reservoirs of electrolyte were used.
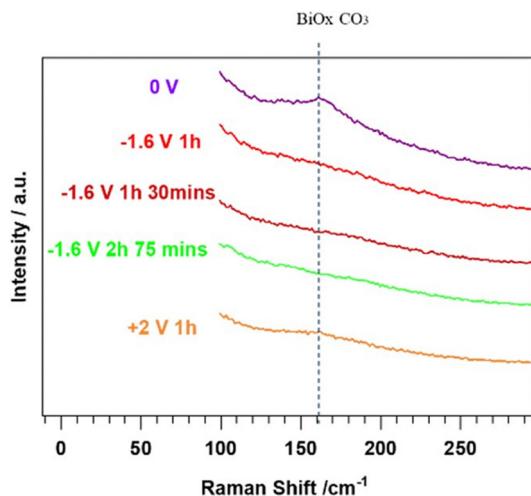
Fig. 9 The changes in the Raman band at 165 cm^{-1} at different applied potential.

bicarbonate solution, which confirmed that the subcarbonate species can be observed due to the interaction of the oxidised Bi surface with (bi)carbonates in the solution. On the other hand, the peak was absent in an experiment with N_2-saturated K_2SO_4 as catholyte.

The *in situ* Raman experiments led to the hypothesis of the significant role of the subcarbonate species as an intermediate in the electrochemical CO_2 reduction of Bi-GDE. During CO_2 electrolysis, the Bi_xO_y surface is reduced, leading to a decreasing affinity of $Bi_2O_2CO_3$ to be formed. Continuous pulsing enables the partial/full re-oxidation of the metal surface, favouring the formation of $Bi_2O_2CO_3$. While *in situ* spectroscopic characterization of Sn during pulsed electrolysis would provide direct confirmation of $Sn(\text{II})/SnO_x$ regeneration, such measurements are beyond the scope of this system-level study. Ongoing work by our group[57] combines *in situ* Raman spectroscopy and DFT analysis to elucidate the re-oxidation mechanisms of Bi and Sn electrodes under pulsed operation. Unlike pulse protocols used primarily for selectivity modulation or flooding mitigation, here pulsing restores Bi/Sn oxidised state and subsequently the reversible regeneration of sub-carbonate species, leading to FA formation.

From our long-term operational data, we identify two primary categories contributing to performance degradation during CO_2 electroreduction: (i) intrinsic catalyst deactivation and (ii) process-induced degradation. These pathways can be distinguished by examining the time-resolved evolution of partial current density in response to applied reactivation strategies, as illustrated in Fig. 10. The reactivation trigger can be associated with a change in process conditions such as pH or conductivity changes, (over)saturation of salts in the electrolyte or accumulation of formate. On the other hand, the reactivation trigger can be linked with intrinsic catalysts or localised phenomena such as morphological changes, gas bubble accumulation, loss of active surface species, and specific crystal orientation of the surface facets. A direct head-to-head control *versus* carbon-supported GDEs was not conducted here; durability challenges
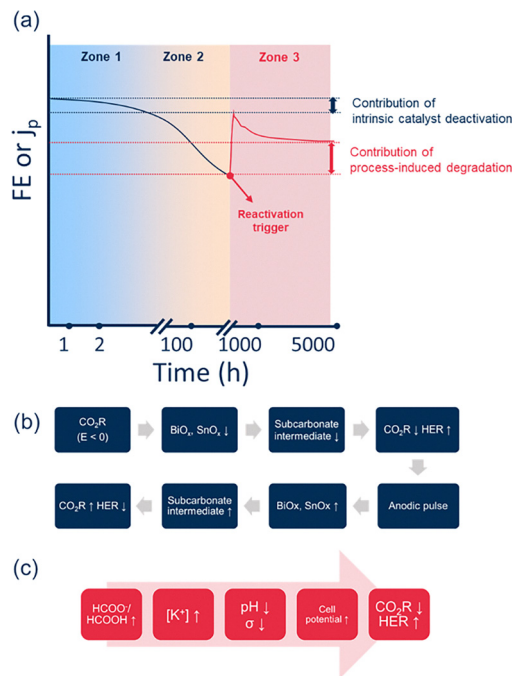

Fig. 10 (a) Schematic representation of different degradation causes; (b) hypothesized flow diagram of phenomena leading to catalyst deactivation/activation and (c) hypothesized flow diagram of phenomena leading to process-induced degradation.

of carbon GDLs (flooding/salt precipitation/corrosion) are well documented and motivate our carbon-free design. For the Sn and Bi GDE systems investigated in this study, we propose mechanistic pathways underpinning both degradation modes: intrinsic catalyst deactivation is depicted in Fig. 10(b), while process-induced degradation is summarised in Fig. 10(c). Differentiating these degradation mechanisms provides a framework to guide mitigation strategies, including tailored electrode design and dynamic process control, to enhance the long-term stability of electrochemical CO_2 reduction systems.

In general, it is proposed that during the initial stages of CO_2 electrolysis, performance degradation is primarily driven by intrinsic catalyst deactivation, corresponding to the end of Zone 1. Over extended operation, however, process-induced degradation mechanisms become increasingly dominant (Zone 2). The duration and onset of these zones are not sharply defined and are influenced by multiple factors, including catalyst robustness, reactor configuration, reservoir volume, and operational parameters. This behavioural trend is representative of relatively mature systems, such as the Sn and Bi GDEs developed in this study. Electrocatalyst screening is often limited to short durations in H-cell setups, typically within Zone 1, where catalyst stability may appear more favourable than in continuous operation. We contend that ultra-high intrinsic selectivity (*e.g.*, FE > 95%) is not always essential; rather, the ability of a catalyst to maintain performance under prolonged and variable operating conditions is of greater practical relevance. The susceptibility of a catalyst to external triggers such as an anodic pulse for our Sn and Bi GDE is a
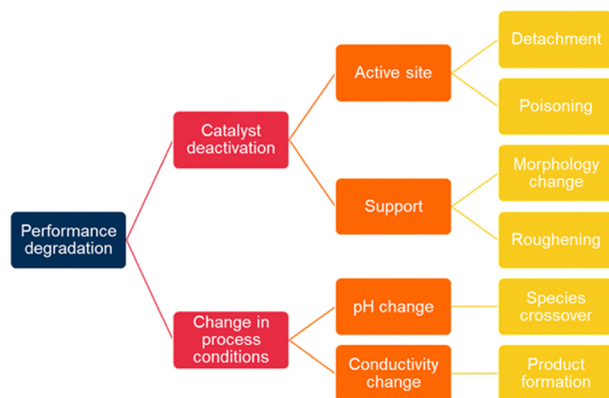
Fig. 11 Schematic of factors responsible for performance degradation in a long-term electrocatalytic process distinguishing between factors related to the electrocatalyst and to a change in process conditions.

more important parameter to extend the durability of the CO_2 electrolysis process. Fig. 11 provides a simplified overview of major issues leading to electrochemical performance degradation during long term operation. We differentiate between factors related to the electrocatalyst itself and factors caused by a change in reaction conditions. As shown, no single mechanism fully accounts for the observed decline; instead, a convergence of intrinsic and extrinsic phenomena often dictates system behaviour over time.

Conclusions

In this study, we present a novel fabrication strategy for robust, carbon-free Bi and Sn gas diffusion electrodes (GDEs), enabling extended ECR in a liquid-fed CO_2 electrolyser. Long-term operation was demonstrated with Bi and Sn GDEs sustaining stable performance over 4000 hours and 1050 hours, respectively, at a current density of 100 mA cm^{-2}, with faradaic efficiencies of $\sim$90% and $\sim$70% for formate/formic acid production Our findings reveal that performance degradation is predominantly influenced by changes in electrolyte properties, specifically pH and conductivity, rather than intrinsic catalyst failure. Through a combination of catholyte management and periodic anodic pulsing, we demonstrate effective reactivation of GDE performance. In particular, anodic pulses appear to promote the regeneration of subcarbonate intermediates, which play a critical role in catalyst selectivity and stability on these electrodes. While gradual performance variations were observed due to electrolyte evolution, the combination of pulsed electrolysis and electrolyte refreshment effectively reactivated the electrodes, maintaining high faradaic efficiency over thousands of hours. By identifying both process- and catalyst-induced degradation pathways, and implementing a strategy to mitigate them, this work provides a pathway for prolonged and efficient CO_2 electrolysis. These insights contribute to the design of durable electrode systems and operational protocols, advancing the industrial viability of ECR technologies within carbon-neutral energy infrastructures.

Author contributions

C. Singh & J. Song carried out the methodology, electrochemical measurements, data analysis and writing – original draft; R. Prasannachandran, A. Grijalvo, J. Shen, Z. Chen carried out the control electrochemical experiments, conducting electrochemical measurement and data analysis; Y. Y. Birdja, J. Vaes and D. Pant acquired funding and were responsible for project administration, supervision, and writing – review & editing. All authors participated in the discussion of the manuscript results.

Conflicts of interest

Three authors (Yuvraj Birdja, Jan Vaes and Deepak Pant) are inventors of the patent EEP4182491B1 "Carbon free gas diffusion electrode" (Granted in July 2025), while five authors (Chandani Singh, Jia Song, Zhiyuan Chen, Yuvraj Birdja, Jan Vaes and Deepak Pant) are inventors on the patent application EP4474526A1 "Re-activation process of gas diffusion electrode" (filed in 2023) and thus declare a competing financial interest due to employment at VITO. The other authors have no competing financial interests.

Data availability

The data supporting the findings of this study are presented in the Figures of the main manuscript and in the accompanying SI. As disclosed in the Conflict-of-Interest statement, the research detailed in this article is associated with two patent applications filed by VITO, which are presently undergoing licensing negotiations. Upon finalization of these agreements, the underlying experimental raw data will be made publicly accessible *via* VITO's official GitHub repositories, which host resources related to their research and development activities: https://github.com/orgs/VITObelgium/repositories. Till then, this data is available from the corresponding author upon reasonable request. Supplementary information (SI) describing the preparation, activation and characterization of electrodes as well as additional results from the long-term operation is available. See DOI: https://doi.org/10.1039/d5ey00330j.

References

1 J. Mertens, C. Breyer, K. Arning, A. Bardow, R. Belmans, A. Dibenedetto, S. Erkman, J. Gripekoven, G. Léonard, S. Nizou, D. Pant, A. S. Reis-Machado, P. Styring, J. Vente, M. Webber and C. J. Sapart, *Joule*, 2023, 7, 442–449.

2 S. Varhade, A. Guruji, C. Singh, G. Cicero, M. García-Melchor, J. Helsen and D. Pant, *ChemElectroChem*, 2024, e202400512.

3 P. Debergh, O. Gutiérrez-Sánchez, M. N. Khan, Y. Y. Birdja, D. Pant and M. Bulut, *ACS Energy Lett.*, 2023, **8**, 3398–3403.

4 D. Ewis, M. Arsalan, M. Khaled, D. Pant, M. M. Ba-Abbad, A. Amhamed and M. H. El-Naas, *Sep. Purif. Technol.*, 2023, **316**, 123811.

5 D. S. Tran, N.-N. Vu, H.-E. Nemamcha, C. Boisvert, U. Legrand, A. G. Fink, F. Navarro-Pardo, C.-T. Dinh and P. Nguyen-Tri, *Coord. Chem. Rev.*, 2025, **524**, 216322.

6 C. Chen, X. Yan, S. Liu, Y. Wu, Q. Wan, X. Sun, Q. Zhu, H. Liu, J. Ma, L. Zheng, H. Wu and B. Han, *Angew. Chem.*, 2020, **132**, 16601–16606.

7 A. Ozden, Y. Wang, F. Li, M. Luo, J. Sisler, A. Thevenon, A. Rosas-Hernández, T. Burdyny, Y. Lum, H. Yadegari, T. Agapie, J. C. Peters, E. H. Sargent and D. Sinton, *Joule*, 2021, **5**, 706–719.

8 E. W. Lees, B. A. W. Mowbray, F. G. L. Parlane and C. P. Berlinguette, *Nat. Rev. Mater.*, 2021, **7**, 55–64.

9 K. Yang, R. Kas, W. A. Smith and T. Burdyny, *ACS Energy Lett.*, 2021, **6**, 33–40.

10 B. van den Bosch, J. Krasovic, B. Rawls and A. L. Jongerius, *Curr. Opin. Green Sustainable Chem.*, 2022, **34**, 100592.

11 M. Sassenburg, R. de Rooij, N. T. Nesbitt, R. Kas, S. Chandrashekar, N. J. Firet, K. Yang, K. Liu, M. A. Blommaert, M. Kolen, D. Ripepi, W. A. Smith and T. Burdyny, *ACS Appl. Energy Mater.*, 2022, **5**, 5983–5994.

12 K. Peramaiah, M. Yi, I. Dutta, S. Chatterjee, H. Zhang, Z. Lai and K.-W. Huang, *Adv. Mater.*, 2024, **36**, 2404980.

13 K. Van Daele, B. De Mot, M. Pupo, N. Daems, D. Pant, R. Kortlever and T. Breugelmans, *ACS Energy Lett.*, 2021, **6**, 4317–4327.

14 K. Fernández-Caso, G. Díaz-Sainz, M. Alvarez-Guerra and A. Irabien, *ACS Energy Lett.*, 2023, **8**, 1992–2024.

15 G. Díaz-Sainz, M. Alvarez-Guerra and A. Irabien, *J. CO2 Util.*, 2022, **56**, 101822.

16 M. Manolova, J. Hildebrand, S. Hertle, Ş. Sörgel, H. Kassner and E. Klemm, *Appl. Sci.*, 2023, **13**, 7471.

17 K. Morishita, T. Murakami, T. Matsumoto, K. Koike, K. Fujii, T. Ogawa and S. Wada, *Jpn J. Appl. Phys.*, 2025, **64**, 04SP61.

18 W. Ma, J. Morales-Vidal, J. Tian, M.-T. Liu, S. Jin, W. Ren, J. Taubmann, C. Chatzichristodoulou, J. Luterbacher, H. M. Chen, N. López and X. Hu, *Nature*, 2025, **641**, 1156–1161.

19 J. A. Abarca, G. Díaz-Sainz, I. Merino-Garcia, G. Beobide, J. Albo and A. Irabien, *J. Environ. Chem. Eng.*, 2023, **11**, 109724.

20 B. N. Khiarak, A. Fell, N. Anand, S. Md Sadaf and C.-T. Dinh, *Catal. Today*, 2024, **426**, 114393.

21 H. Yang, J. J. Kaczur, S. D. Sajjad and R. I. Masel, *J. CO2 Util.*, 2017, **20**, 208–217.

22 L. Li, A. Ozden, S. Guo, F. P. Garcia de Arquer, C. Wang, M. Zhang, J. Zhang, H. Jiang, W. Wang, H. Dong, D. Sinton, E. H. Sargent and M. Zhong, *Nat. Commun.*, 2021, **12**, 5223.

23 Y. Y. Birdja and J. Vaes, *ChemElectroChem*, 2020, **7**, 4713–4717.

24 B. Belsa, L. Xia and F. P. García de Arquer, *ACS Energy Lett.*, 2024, **9**, 4293–4305.

25 A. Silveira Sbrice Pinto, N. Gulpinar, F. Liu, E. Gibson, L. Fuller and P. Souter, *ACS Sustainable Resour. Manage.*, 2025, **2**, 733–743.

26 J. A. Abarca, M. Coz-Cruz, M. Alvarez-Guerra, G. Díaz-Sainz and A. Irabien, *Electrochim. Acta*, 2025, **525**, 146182.

27 A. Löwe, M. Schmidt, F. Bienen, D. Kopljar, N. Wagner and E. Klemm, *ACS Sustainable Chem. Eng.*, 2021, **9**, 4213–4223.

28 B. Jacobs; D. Pant, D. Van Houtevn, E. Maes, J. Vaes and Y. Y. Birdja, Carbon-free gas diffusion electrode, *EP EP 4182491 B1*, European Patent Office, Granted July 2, 2025.

29 T. Li, E. W. Lees, M. Goldman, D. A. Salvatore, D. M. Weekes and C. P. Berlinguette, *Joule*, 2019, **3**, 1487–1497.

30 M. Ramdin, A. R. T. Morrison, M. de Groen, R. van Haperen, R. de Kler, L. J. P. van den Broeke, J. P. M. Trusler, W. de Jong and T. J. H. Vlugt, *Ind. Eng. Chem. Res.*, 2019, **58**, 1834–1847.

31 S. J. Folkman, J. González-Cobos, S. Giancola, I. Sánchez-Molina and J. R. Galán-Mascarós, *Molecules*, 2021, **26**, 4756.

32 M. Sassenburg, M. Kelly, S. Subramanian, W. A. Smith and T. Burdyny, *ACS Energy Lett.*, 2023, **8**, 321–331.

33 M. Sassenburg, R. de Rooij, N. T. Nesbitt, R. Kas, S. Chandrashekar, N. J. Firet, K. Yang, K. Liu, M. A. Blommaert, M. Kolen, D. Ripepi, W. A. Smith and T. Burdyny, *ACS Appl. Energy Mater.*, 2022, **5**, 5983–5994.

34 Y. Xu, J. P. Edwards, S. Liu, R. K. Miao, J. E. Huang, C. M. Gabardo, C. P. O'Brien, J. Li, E. H. Sargent and D. Sinton, *ACS Energy Lett.*, 2021, **6**, 809–815.

35 E. N. Butt, J. T. Padding and R. Hartkamp, *ACS Electrochem.*, 2025, **1**, 2475–2483.

36 F. Dattila, R. Garcia-Muelas and N. López, *ACS Energy Lett.*, 2020, **5**, 3176–3184.

37 B. Kumar, J. P. Brian, V. Atla, S. Kumari, K. A. Bertram, R. T. White and J. M. Spurgeon, *ACS Catal.*, 2016, **6**, 4739–4745.

38 A. Herzog, M. Lopez Luna, H. S. Jeon, C. Rettenmaier, P. Grosse, A. Bergmann and B. Roldan Cuenya, *Nat. Commun.*, 2024, **15**, 3986.

39 W. Xi, H. Zhou, P. Yang, H. Huang, J. Tian, M. Ratova and D. Wu, *ACS Catal.*, 2024, **14**, 13697–13722.

40 J. Kok, J. de Ruiter, W. van der Stam and T. Burdyny, *J. Am. Chem. Soc.*, 2024, **146**, 19509–19520.

41 T. Ito, J. Raj, T. Zhang, S. Roy and J. Wu, *EES Catal.*, 2024, **2**, 997–1005.

42 H. S. Jeon, J. Timoshenko, C. Rettenmaier, A. Herzog, A. Yoon, S. W. Chee, S. Oener, U. Hejral, F. T. Haase and B. Roldan Cuenya, *J. Am. Chem. Soc.*, 2021, **143**, 7578–7587.

43 N. Mikami, K. Morishita, T. Murakami, T. Hosobata, Y. Yamagata, T. Ogawa, Y. Mukouyama, S. Nakanishi, J. W. Ager, K. Fujii and S. Wada, *ACS Energy Lett.*, 2024, 4225–4232.

44 Y. L. Chung, S. Kim, Y. Lee, D. T. Wijaya, C. W. Lee, K. Jin and J. Na, *iScience*, 2024, **27**(8), 110383.

45 L. C. Tănase, M. J. Prieto, L. de Souza Caldas, A. Tiwari, F. Scholten, P. Grosse, A. Martini, J. Timoshenko, T. Schmidt and B. Roldan Cuenya, *Nat. Catal.*, 2025, **8**, 881–890.

46 K. Ye, T.-W. Jiang, H. D. Jung, P. Shen, S. M. Jang, Z. Weng, S. Back, W.-B. Cai and K. Jiang, *Nat. Commun.*, 2024, **15**, 9781.

47 Y. Jännsch, J. J. Leung, M. Hämmerle, E. Magori, K. Wiesner-Fleischer, E. Simon, M. Fleischer and R. Moos, *Electrochem. Commun.*, 2020, **121**, 106861.

48 Y. Zhang, X. Zhang, Y. Ling, F. Li, A. M. Bond and J. Zhang, *Angew. Chem., Int. Ed.*, 2018, **57**, 13283–13287.

49 R. Casebolt, K. Levine, J. Suntivich and T. Hanrath, *Joule*, 2021, **5**, 1987–2026.

50 Y. Zhang, X. Zhang, Y. Ling, F. Li, A. M. Bond and J. Zhang, *Angew. Chem., Int. Ed.*, 2018, **57**, 13283–13287.

51 Y. Shi, C. F. Wen, X. Wu, J. Y. Zhao, F. Mao, P. F. Liu and H. G. Yang, *Mater. Chem. Front.*, 2022, **6**, 1091–1097.

52 L. G. Puppin, M. Khalid, G. T. T. Da Silva, C. Ribeiro, H. Varela and O. F. Lopes, *J. Mater. Res.*, 2020, **35**, 272–280.

53 Y. Wang, B. Wang, W. Jiang, Z. Liu, J. Zhang, L. Gao and W. Yao, *Nano Res.*, 2022, **15**, 2919–2927.

54 D. Yao, C. Tang, A. Vasileff, X. Zhi, Y. Jiao and S. Z. Qiao, *Angew. Chem., Int. Ed.*, 2021, **60**, 18178–18184.

55 X. An, S. Li, X. Hao, X. Du, T. Yu, Z. Wang, X. Hao, A. Abdula and G. Guan, *Sustainable Energy Fuels*, 2020, **4**, 2831–2840.

56 Y. Zhou, P. Yan, J. Jia, S. Zhang, X. Zheng, L. Zhang, B. Zhang, J. Chen, W. Hao, G. Chen, Q. Xu and B. Han, *J. Mater. Chem. A*, 2020, **8**, 13320–13327.

57 R. Prasannachandran, D. Cornil, Z. Chen, D. Beljonne and Y. Y. Birdja, *Restoring Formate Selectivity: In Situ Raman Study of Deactivated Electrodes for CO2 electroreduction*, Under preparation.